Growth and Microstructure of Nanoscale Amorphous Carbon Nitride Films Deposited by Electron Beam Irradiation of 1,2-Diaminopropane

Joshua D. Wnuk,[†] Justin M. Gorham,[†] and D. Howard Fairbrother*[,†,‡]

Departments of Chemistry and Materials Science and Engineering, Johns Hopkins University, Baltimore, Maryland 21218

Received: February 2, 2009; Revised Manuscript Received: May 5, 2009

The deposition and microstructure of nanoscale nitrogen containing carbon films produced by irradiating adsorbed 1,2-diaminopropane (1,2-DAP) molecules with >40 eV electrons has been studied. The growth rate of films deposited in the presence of a constant partial pressure of 1,2-DAP was directly proportional to the flux of both precursor 1,2-DAP molecules and the incident electrons, consistent with an electron beam induced deposition (EBID) process. Deposited films were highly textured and weakly adhered to the polycrystalline Au substrate. Complementary information on the electron stimulated decomposition of the precursor and the accompanying film growth was obtained from experiments performed under ultrahigh vacuum (UHV) on nanometer scale thick films of 1,2-DAP. Results from these UHV studies were consistent with the idea that decomposition was initiated by secondary electrons, produced by the interaction of the primary electron beam with the adsorbate layer and the substrate. Reactions of these low energy secondary electrons with adsorbed 1,2-DAP molecules were responsible for dehydrogenation as well as film growth. For prolonged electron exposures nitrile species were produced, supporting the idea that changes in the film's microstructure and chemical composition were due to the effects of C−H and N−H, rather than C−C or C−N, bond cleavage. Collectively, our results indicate that EBID initially leads to the formation of a hydrogenated carbon nitride (a:C−N(H)) film. Further electron stimulated dehydrogenation ultimately yields an amorphous carbon−nitride film (a:C−N).

Downloaded by JOHNS HOPKINS UNIV on July 14, 2009
Published on June 15, 2009 on http://pubs.acs.org | doi: 10.1021/jp900966m

I. Introduction

Amorphous carbon nitride (a:C−N) and hydrogenated carbon nitride (a:C−N(H)) films are becoming an increasingly important and widely used class of materials due to the beneficial effects that nitrogen incorporation has on the wear resistance,[1−3] biocompatibility, adhesion characteristics,[4] optical/electronic properties,[5−7] and thermal stability of amorphous carbon films.[8] Indeed, nitrogen doped carbonaceous films are replacing carbonaceous films as nanometer scale (<10 nm), wear-resistant hard disk coatings, and recorder heads in magnetic storage devices.[9] Hydrogenated carbon nitride films also exhibit remarkable field emission properties[10,11] and are being considered as cold cathode materials in vacuum microelectronics and flat panel display technologies.[12] *It should be noted that in this manuscript we use the term carbon nitride film to describe any carbon-based film that also contains nitrogen atoms (and possibly hydrogen).*

The deposition of amorphous carbon nitride thin films is typically accomplished in low pressure, plasma environments.[13−18] Under these conditions, growth is a consequence of complex surface reactions involving an array of reactive species, including ions, radicals, photons, and electrons, the later including secondary electrons produced by the interaction of incident photons and electrons with the substrate.[19] To date, uncovering the specific role that individual species, such as electrons, play in controlling the deposition rate as well as the microstructure of amorphous carbon nitride thin films has been hampered by the complexity of the gas phase medium.[20−22] Thus, although the properties of carbon nitride films are known to be strongly dependent upon macroscopic deposition parameters (input power, gas phase composition),[23−26] only a few of the specific surface processes involved in film growth have been identified.[27]

The irradiation of solid substrates in the presence of background hydrocarbons by electrons has been identified as the reason for the unwanted formation of amorphous carbonaceous films on windows and lenses in electron microscopes.[28−30] This same electron beam induced deposition (EBID) process has, however, recently been exploited for the controlled deposition of two and three-dimenisonal nanostructures,[31−42] where the inherent flexibility and focusing capabilities of electrons allows nanostructures to be patterned without resists. In the context of amorphous carbon nitride thin films, EBID could represent a new route for the controlled deposition of nanoscale protective coatings and electron field emission nanotips. The growth rate, composition, and structure of EBID materials are a function of the incident beam energy, current density, and spot size as well as the chemical composition and pressure of the gas phase precursor.[35,36,43−46] However, attempts to improve existing processes have to date been hindered by a lack of molecular-level understanding regarding the electron-stimulated reactions and chemical transformations that underpin EBID.

In the present study, we have investigated the electron-induced deposition of amorphous carbon nitride films using 1,2-diaminopropane (1,2-DAP) as a model precursor. The decision to use 1,2-DAP was based on its desirable physical properties (liquid at STP with a boiling point of 120 °C) and commercial availability. The relatively high fraction of nitrogen atoms (N/C = 2:3) in 1,2-DAP ($CH_3CH(NH_2)CH_2NH_2$) also facilitated a determination of the concentration and distribution of nitrogen-

* To whom correspondence should be addressed. E-mail: howardf@jhu.edu.
† Department of Chemistry.
‡ Department of Materials Science and Engineering.

10.1021/jp900966m CCC: $40.75 © 2009 American Chemical Society
Published on Web 06/15/2009

containing species in the deposited films. In the presence of a constant partial pressure of 1,2-DAP, the EBID growth kinetics, structure, and chemical composition of amorphous carbon nitride films deposited on a solid substrate were examined. To provide complementary information on electron stimulated reaction mechanisms, growth processes, and the influence of irradiation time on the film's structure, separate experiments were performed under ultrahigh vacuum (UHV) on nanometer scale thick 1,2-DAP films. The value of this UHV experimental approach to probe electron-mediated processes has been demonstrated in recent studies relevant to atmospheric chemistry,[47−49] astrochemistry,[50,51] astrobiology,[52] thin film modification,[53−57] and radiation damage to biologically relevant molecules.[55,58,59]

II. Experimental Section

EBID studies were conducted using two different types of experiments.[60] In one approach, deposition was accomplished at room temperature using a focused electron beam (radius ≈ 2 μm) in the presence of a constant pressure of 1,2-DAP, $CH_3CH(NH_2)CH_2NH_2$ (Sigma-Aldrich). The growth kinetics and properties of these films were studied using a combination of Auger electron spectroscopy (AES) and atomic force microscopy (AFM). These studies were complemented by UHV experiments performed on multilayer films of 1,2-DAP deposited at low temperature (≈100 K) using a broad beam electron source. In these studies, electron induced reactions were probed by reflection absorption infrared spectroscopy (RAIRS) in one UHV chamber[47,48] and X-ray photoelectron spectroscopy (XPS) and mass spectrometry (MS) in a second UHV chamber.[60−62] Unless noted, the incident electron energy was 1.5 keV. In all of the experiments described, Au was used as the substrate. This decision was based on the ease of obtaining clean Au surfaces by Ar^+ sputtering, the chemical inertness of Au toward adsorbed 1,2-DAP, and the high reflectivity of polished Au substrates.

Films Deposited in a Partial Pressure of 1,2-DAP. In these experiments, amorphous carbon nitride films were deposited by irradiating a Au substrate with 1.5 keV electrons generated from a PHI 610 AES spectrometer[63] in the presence of a constant partial pressure of 1,2-DAP. Experiments were performed in a UHV system ($P_{base} < 2 \times 10^{-9}$ Torr), equipped with capabilities for in situ scanning AES, secondary electron detection (SED) and mass spectrometry (MS, Quadstar Prisma QMS 200), a PHI 04-303 ion gun for sample cleaning, and a UHV-compatible leak valve for gas dosing. Film growth was performed on polycrystalline Au substrates (∼200 nm thick) that had been grown on a Si(100) wafer by thermal evaporation, following the deposition of a ∼20 nm thick Cr seed layer. Prior to deposition, the Au substrate was introduced into the UHV chamber and sputter cleaned with 2 keV Ar^+ ions to remove any residual carbon contamination, as verified by AES.

1,2-DAP was stored as a liquid in a sealed glass-to-metal container attached to an external gas manifold, which was frequently evacuated via an independent pump to remove atmospheric impurities; gas purity was routinely verified by mass spectrometry. During EBID, the background pressure of 1,2-DAP in the UHV chamber was maintained at $\sim 5 \times 10^{-7}$ Torr; to enhance the local pressure of 1,2-DAP, a stainless steel tube was used to direct the gas flow onto the Au surface. To induce film growth in the presence of a partial pressure of 1,2-DAP, 1.5 keV electrons, generated from the LaB_6 filament used for AES, were rastered over a known area of the Au substrate. During deposition, the flux of electrons at the Au substrate was monitored by recording the target current.

Film Characterization. The location and two-dimensional shape of films deposited by electron irradiation were monitored using SED, while the film's chemical composition and thickness were quantified by AES. Morphological analysis of selected films was also performed ex situ using AFM. In these experiments, the substrate was removed from the vacuum chamber and adhered to the AFM sample plate using double-sided carbon tape. Au substrates used for AFM analysis were also scribed to provide physical markers, which were used in conjunction with SED images, to help locate the deposited film's position with the optical microscope attached to the AFM. Images acquired by AFM were taken using a PicoSPM LE (Agilent Technologies) operating in magnetic tapping mode using Co−Cr tips obtained from MikroMasch (NSC18). All image rendering and height measurements were performed utilizing commercially available software from Agilent Technologies.

Electron Stimulated Reactions in Nanometer-Scale Thick 1,2-DAP Films. The effect of electron irradiation on nanometer scale thick films of 1,2-DAP was studied by XPS and MS in an UHV chamber with a base pressure of $\sim 3 \times 10^{-9}$ Torr.[60] In these experiments, the Au substrate was attached to a Ta sample holder mounted at the end of a manipulator arm with capabilities for *XYZ* translation and 360° rotation. Routine sample cleaning, which included the removal of electron deposited material, was performed by rastering the substrate with 4 keV Ar^+ ions until XPS confirmed the substrate was >99% Au. A type K thermocouple, adhered to the underside of the Ta holder, was used to monitor the substrate temperature. The effect of electron irradiation on the surface composition was monitored by XPS using Mg Kα radiation (1253.6 eV). Ejected photoelectrons were analyzed by a multichannel hemispherical analyzer operating at a pass energy of 22.36 eV and a step size of 0.125 eV. All XPS peak positions reported in this study have been referenced to the Au($4f_{7/2}$) peak at 83.8 eV. Mass spectra were obtained using a QMS (Stanford Research; RGA 200: electron energy 70 eV) positioned ∼12 cm from the substrate and in a direct line-of-sight.

RAIRS experiments were performed in a separate UHV ($P_{base} = \sim 4 \times 10^{-9}$ Torr) chamber fitted with differentially pumped ZnSe windows. A mirrored polycrystalline Au substrate (∼5.7 cm^2) was mounted onto a manipulator arm capable of *XYZ* translation and 360° rotation, using a Cu support. A type K thermocouple was attached to the underside of the substrate to monitor temperature. To acquire vibrational spectra, a Mattson Infinity Series Fourier Transform infrared spectrometer was used in conjunction with an external narrow band InSb detector (1900−4000 cm^{-1}) operating at a resolution of 4 cm^{-1}.

Film Deposition. For XPS, MS, and RAIRS studies, nanometer-scale thick 1,2-DAP films were deposited by molecularly adsorbing 1,2-DAP onto a cooled Au substrate (∼100 K). In the XPS/MS chamber, 1,2-DAP was directionally dosed through a stainless steel tube. In the RAIRS chamber, gas adsorption onto the cooled substrate was accomplished by backfilling the chamber with 8×10^{-7} Torr of 1,2-DAP for a controlled exposure time. Film thicknesses in the XPS and MS experiments were determined by measuring the attenuation of the XPS signal from the Au(4f) photoelectrons following 1,2-DAP adsorption. In RAIRS experiments, the film thickness was not quantitatively determined.

Electron Source. A commercial flood gun (Specs 15/40) was used as a source of broad electron beam irradiation in XPS, MS, and RAIRS experiments.[60] During irradiation, substrates were positioned in a line of sight to the electron source at a distance of ∼6 cm. The flood gun produces an electron beam with an ≈1.0 cm full width at half-maximum at a distance of 2.0 cm, providing a reasonably uniform flux of electrons at the

Downloaded by JOHNS HOPKINS UNIV on July 14, 2009
Published on June 15, 2009 on http://pubs.acs.org | doi: 10.1021/jp900966m

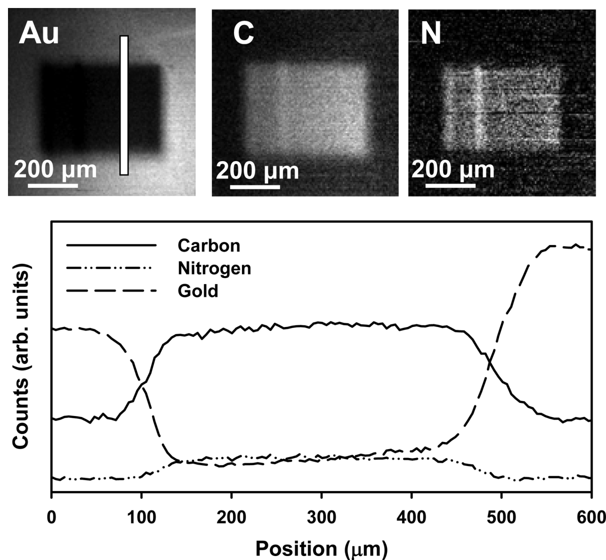

Figure 1. (top) Gold, carbon, and nitrogen AES maps of an amorphous carbon nitride film deposited by electron irradiation (0.095 μA, 5×10^{-7} Torr, 180 min) of 1,2-diaminopropane. (bottom) Line scan showing the variation in gold, carbon, and nitrogen AES signals along the white line indicated in the gold AES map.

Downloaded by JOHNS HOPKINS UNIV on July 14, 2009
Published on June 15, 2009 on http://pubs.acs.org | doi: 10.1021/jp900966m

surface. Unless noted, the incident electron energy was 1.5 keV. The electron energy was calculated from the sum of the electron energy generated by the flood gun and the positive bias applied to the substrate. The target current was measured to ground via a digital ammeter placed in series with an external voltage source.

III. Results

Figure 1 shows the Au, C, and N Auger maps obtained after an $\approx 350 \times 500$ μm area of an initially clean Au substrate was rastered by 1.5 keV electrons in the presence of a constant partial pressure of 1,2-DAP (5×10^{-7} Torr) and fixed target current/electron flux (0.095 μA) for 180 min. A measurable increase in the C and N AES signals is observed within the irradiated area, consistent with the electron-induced deposition of a carbon nitride thin film. Conversely, the Au AES signal is attenuated within the irradiated area due to the EBID overlayer. The presence of C and N within the irradiated area is also supported by the AES line scan results.

In Figure 2, separate AES experiments were performed to investigate the influence of 1,2-DAP exposure time (Figure 2a) and the target current/electron flux (Figure 2b) on the thickness of the EBID deposit. In this analysis, we utilized the well-known relationship between film thickness and the AES signal associated with the underlying substrate (Au)

$$\text{film thickness} \propto \ln (\mathrm{Au_0}/\mathrm{Au_f})$$

where Au_0 and Au_f are the Au AES signal intensities before and after film deposition, respectively.

In Figure 3, AFM was used to probe the surface structure of an amorphous carbon nitride thin film that had been electron beam deposited onto a Au substrate. To facilitate a direct comparison of the film's topography to that of the underlying Au substrate, the AFM tip was used to physically remove a small portion of the film and expose the underlying substrate. This was accomplished by minimizing the tip oscillation and increasing the applied load within a square region of the image,[64] as shown in Figure 3a. A higher magnification AFM image that provides a more detailed comparison of the film's morphology to that of the substrate is shown in Figure 3b.

Figure 4a shows the MS fragmentation pattern of gas phase 1,2-DAP, measured under UHV. In contrast, Figure 4b shows the volatile products produced when physisorbed 1,2-DAP molecules are exposed to electron irradiation. For gas phase 1,2-DAP (Figure 4a), prominent peaks are observed at m/z = 44 and m/z = 30, corresponding to $C_2H_6N^+$ and CH_4N^+ fragments, respectively; minor peaks at m/z = 2 (hydrogen) and m/z = 74 (parent peak; $C_3H_{10}N_2^+$) are also observed. The spectra shown in Figure 4a is consistent with the reported fragmentation pattern of gas phase 1,2-DAP[65] and with the fragmentation pattern expected for amines.[66] In contrast to Figure 4a, hydrogen is the dominant volatile species produced when 1,2-DAP multilayers are irradiated by 1.5 keV electrons (Figure 4b). Because hydrogen is also produced from the electron source, control experiments were performed to analyze the gas phase species produced when the Au substrate was irradiated by electrons in the presence and absence of adsorbed 1,2-DAP. Results from these studies confirmed that the overwhelming majority of the hydrogen signal observed in Figure 4b emanates from electron stimulated reactions of adsorbed 1,2-DAP. It should be noted that a detailed kinetic analysis of the hydrogen signal observed during electron irradiation was precluded by the relatively poor pumping speed of hydrogen by turbomolecular pumps, coupled with the time-dependent hydrogen signal produced by the flood gun. Minor peaks at m/z = 15−17 observed during electron irradiation of adsorbed 1,2-DAP multilayers are ascribed to methane and ammonia, while the peak at m/z = 28 could either be the result of nitrogen production or a reflection of residual nitrogen or carbon monoxide in the UHV chamber.

Figure 5 illustrates the changes that occur in the N−H and C−H stretching regions of the IR spectrum when 1,2-DAP multilayers are exposed to electron irradiation, measured for different combinations of electron flux and incident electron energy. Prior to electron irradiation, each deposited film exhibited two vibrational bands characteristic of the N−H (3400−3120 cm^{-1}) and C−H (3000−2775 cm^{-1}) stretching modes of 1,2-DAP.[67] The initial thickness of the three films (within 3%, as measured by the C−H and N−H IR peak areas) is also comparable. For each 1,2-DAP multilayer, electron irradiation produces a systematic decrease in intensity within the N−H and C−H stretching bands (Figure 5), a broadening of the spectral envelopes and a reduction in the resolution of individual peaks within the IR bands. For sufficiently long periods of electron irradiation, there is no evidence of any residual C−H and N−H bonds within any of the films, as measured by IR spectroscopy.

A comparison of Figure 5a, b, and c reveals that the rate of loss of C−H and N−H bonds from the film is sensitive to both the electron flux and the incident electron energy. For example, a comparison of Figures 5a and 5b demonstrates that the loss of IR intensity in the C−H and N−H stretching regions occurs more rapidly when the target current is increased from 10 to 20 μA. Thus, in Figure 5b there is no observable intensity in the C−H or N−H stretching regions after 600 min of irradiation, while for the same exposure time spectral intensity in both regions can be discerned in Figure 5a. A similar comparison between Figures 5b and 5c indicates that when the incident electron energy decreases from 1.5 keV to 200 eV the rate of loss of IR intensity in the C−H and N−H stretching regions increases for the same incident electron flux.

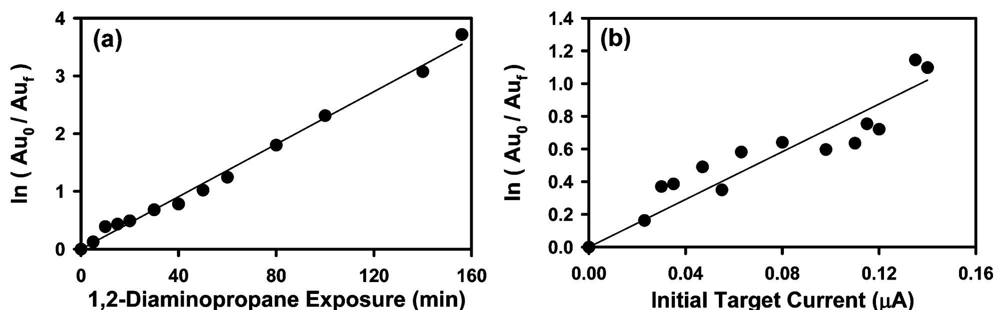

Figure 2. Influence of growth conditions on the film thickness measured by the change in the gold AES signal before (Au_0) and after (Au_f) deposition. Film thickness measured as a function of (a) 1,2-diaminopropane exposure time in the presence of a constant target current (~0.05 μA) and (b) initial target current for a constant 1,2-diaminopropane exposure (20 min). In both (a) and (b), the partial pressure of 1,2-diaminopropane was held constant (5×10^{-7} Torr).

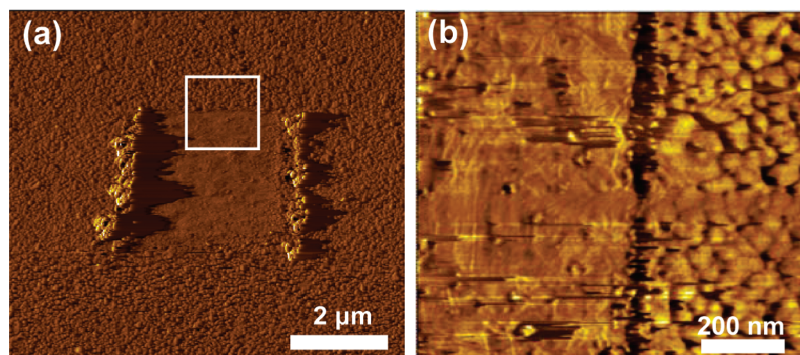

Figure 3. (a) AFM image showing the structure of an electron beam deposited amorphous carbon nitride film grown on a gold substrate. In the center of the image the oscillation amplitude set point of the tip had been decreased to physically remove the deposit. (b) Rotated (90°) AFM image of the region indicated by the white box, showing a more detailed view of the interface between the gold substrate (left) and the deposited film (right).

Downloaded by JOHNS HOPKINS UNIV on July 14, 2009
Published on June 15, 2009 on http://pubs.acs.org | doi: 10.1021/jp900966m

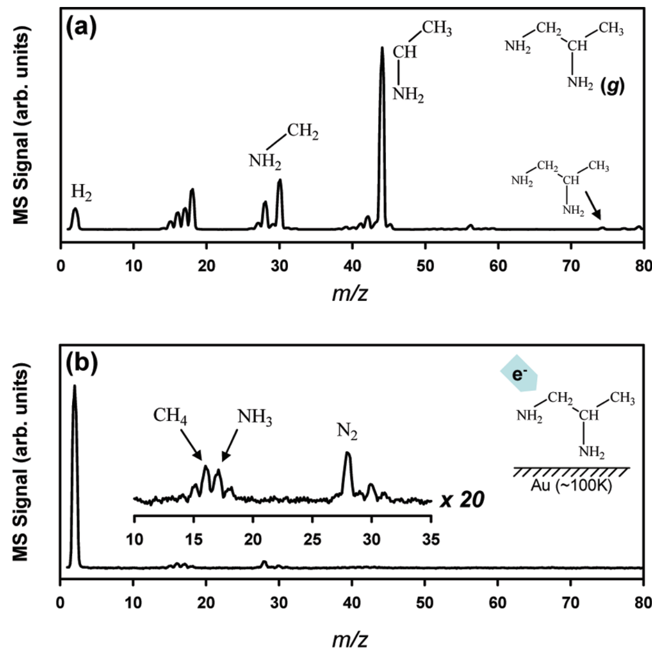

Figure 4. Mass spectra (0–80 a.m.u.) of (a) gas phase 1,2-diaminopropane (70 eV impact energy) and (b) volatile species produced by electron irradiation (1.5 keV; 25 μA) of 1,2-diaminopropane adsorbed onto Au at ~100 K.

Figure 6 shows how the inverse of the irradiation time taken for the C–H (closed triangles) and N–H (open squares) IR bands to decrease to half of their initial values ($1/t_{1/2}$) varies as a function of (a) the target current and (b) the incident electron energy. Figure 6a reveals that for both C–H and N–H IR bands, $1/t_{1/2}$ is directly proportional to the incident electron flux. In Figure 6b the variation in $1/t_{1/2}$ for both C–H and N–H IR bands as a function of the electron's incident kinetic energy (plotted on a log scale) are shown. Analysis of Figure 6b reveals that $1/t_{1/2}$ for both C–H and N–H IR bands vary smoothly with the incident electron energy, exhibiting a maximum at ≈200 eV.

Figure 7a shows a representative example of the how the IR region between 2100–2200 cm^{-1} varies as a function of irradiation time for 1,2-DAP multilayers exposed to 1.5 keV electrons. For the as-deposited 1,2-DAP film and for comparatively short irradiation times there is no evidence of any spectral intensity within this region. However, after 120 s of electron irradiation evidence of a new vibrational band at ≈2155 cm^{-1} can be observed in Figure 7a. Based on the peak position, this new spectral feature is assigned to the stretching band of a nitrile (C≡N) species.[68–70] In Figure 7b, the integrated IR area of the nitrile band has been plotted as a function of the irradiation time. For each RAIRS experiment, the appearance of nitrile species within the adsorbate layer was characterized by an induction time (≈100 s in Figure 7a), while for longer irradiation times the concentration of these species increases with increasing irradiation time before reaching a plateau.

In Figure 8, the effect of electron irradiation on an ≈3.3 nm thick layer of adsorbed 1,2-DAP molecules, as measured by XPS, is shown. Prior to irradiation, single well-defined peaks at 286.8 and 400.2 eV are observed in the C(1s) and N(1s) regions, respectively (Figure 8a), consistent with the XPS spectra of amines.[71] Furthermore, the ratio of nitrogen to carbon in the film, measured by integrating the respective XPS peaks and correcting for the relative sensitivity factors, is 2:3, consistent with the molecular formula of 1,2-DAP. Following an electron exposure sufficient to remove all of the N–H and C–H bonds

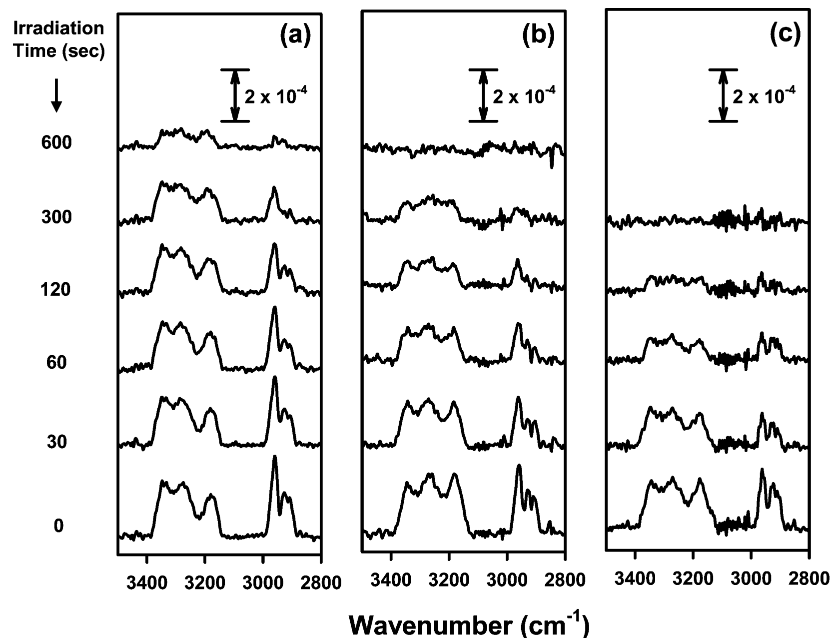

Figure 5. Evolution of the N−H (3400−3120 cm^{-1}) and C−H (3000−2800 cm^{-1}) IR stretching regions for 1,2-diaminopropane multilayers exposed to electron irradiation under three different reaction conditions as characterized by the target current and incident electron energy; (a) 10 μA; 1.5 keV, (b) 20 μA; 1.5 keV, (c) 20 μA; 200 eV. Each RAIR spectra was ratioed to the gold substrate before film deposition.

Downloaded by JOHNS HOPKINS UNIV on July 14, 2009
Published on June 15, 2009 on http://pubs.acs.org | doi: 10.1021/jp900966m

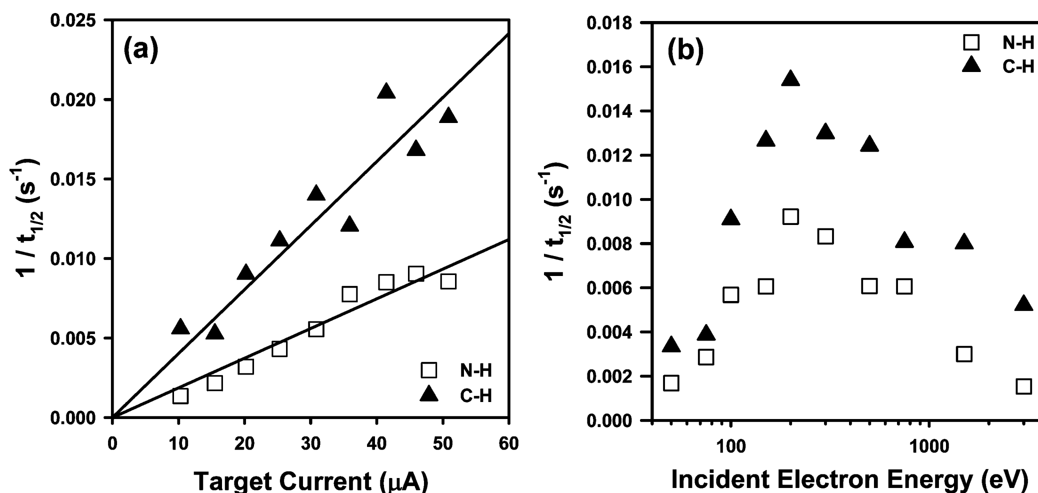

Figure 6. Influence of (a) target current and (b) incident electron energy on the rate of C−H (▲) and N−H (□) bond cleavage from 1,2-diaminopropane multilayers. The rate of C−H and N−H bond cleavage is represented on the *y*-axis as the time taken for the respective IR band intensities to decrease to half of their initial values ($1/t_{1/2}$; see text for details). In the energy-dependent experiments, the target current was maintained at 20 μA.

from the adsorbate layer (as determined by RAIRS), the spectral envelopes in both the C(1s) and N(1s) regions have broadened considerably (compare Figures 8a and 8b). No attempt to fit the C(1s) or N(1s) regions after irradiation has been made due to the ambiguous fits that are obtained. This reflects the significant differences in literature values for assigned peak positions and full width half-maximum values for different CN species.[72−74] Despite the changes in the peak shapes, however, both the C(1s) and N(1s) peak areas remain virtually unchanged after irradiation (<1% difference compared to the native film), although the substrate Au(4f) photoelectron signal increases significantly after electron irradiation (compare Figures 8a and 8b). Following electron irradiation and subsequent XPS analysis, the Au substrate was warmed to room temperature and the adlayer reanalyzed with XPS. This annealing process did not produce any measurable change in the C(1s) or N(1s) line shape or integrated areas. In the absence of electron irradiation, however, all of the C(1s) and N(1s) signal intensity was lost upon annealing 1,2-DAP multilayers to room temperature.

IV. Discussion

The discussion is organized as follows: First, the growth kinetics and structure of carbon nitride films deposited with a focused electron beam in the presence of a constant partial pressure of 1,2-DAP are discussed. Then, experiments performed under UHV conditions on nanometer scale thick films of condensed 1,2-DAP molecules exposed to broad beam electron irradiation are described. Results from these UHV studies are used as the basis to understand how adsorbed 1,2-DAP molecules decompose under the influence of electron irradiation as well as the reactions involved in the growth of the amorphous carbon nitride films and the evolution of the film's microstruc-

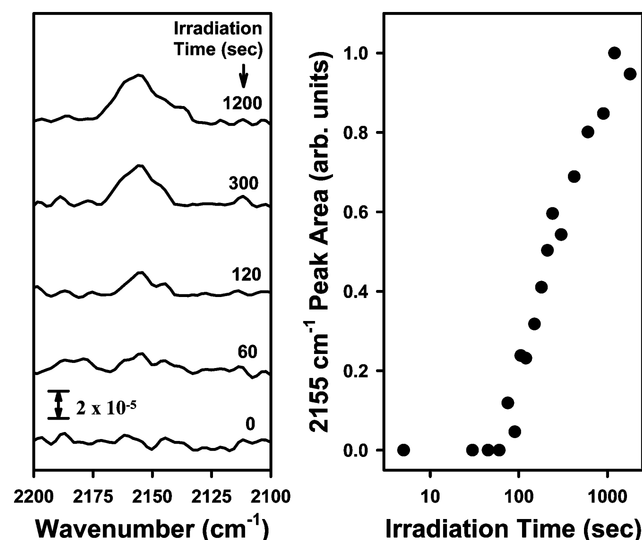

Figure 7. (a) Evolution of the spectral region between 2100 and 2200 cm^{-1} during electron irradiation (36 μA, 1.5 keV) of adsorbed 1,2-diaminopropane. (b) Integrated area of the ~2155 cm^{-1} IR feature as a function of electron irradiation time (plotted on a log scale).

Downloaded by JOHNS HOPKINS UNIV on July 14, 2009
Published on June 15, 2009 on http://pubs.acs.org | doi: 10.1021/jp900966m

ture. Implications of results obtained in the UHV studies as they pertain to EBID of amorphous carbon nitride films are also considered.

Film's Deposited in the Presence of a Constant Partial Pressure of 1,2-DAP. Collectively, the AES data, shown in Figure 1 as well as the SED image shown in Figure 1 of the Supporting Information, demonstrate that amorphous carbon nitride films are deposited when Au substrates are irradiated by 1.5 keV electrons in the presence of 1,2-DAP. Within the deposit, the relative uniformity of the film's chemical composition and thickness is highlighted by the nearly constant C, N, and Au signals in the AES line scan (Figure 1b). Closer inspection of the C and N AES maps shown in Figure 1a reveals that within the irradiated area two vertical stripes can be resolved. Both regions exhibit enhanced C and N AES signal intensities (and a reduced signal intensity in the Au AES map), consistent with the idea that these vertical regions were formed because they were exposed to a higher dose of incident electrons as the focused electron beam was rastered across the surface.

Figure 2 demonstrates that the growth rate of the amorphous carbon nitride films was proportional to both the partial pressure of 1,2-DAP molecules ($P_{1,2\text{-DAP}}$) and the flux of electrons, as measured by the target current at the surface (e^{-}_{flux}). Thus, the overall growth kinetics can be expressed as

$$\text{growth rate} \propto P_{1,2\text{-DAP}} \times e^{-}_{\text{flux}}$$

Such a relationship is typical for EBID, where film growth is mediated by a one electron process that initiates the decomposition of transiently adsorbed precursor molecules into species that remain bound to the substrate.[44,75] Because the steady state concentration of adsorbed precursor molecules (θ) is $\ll 1$, θ will be directly proportional to $P_{1,2\text{-DAP}}$. Structural characterization of the films by AFM (Figure 3) reveals that the deposits are highly textured and significantly rougher than the Au substrate. The fact that the deposited films could be removed by the AFM tip indicates a relatively weak adherence to the Au substrate.

Electron-Induced Chemistry in Nanometer Thick 1,2-DAP Films. In Figures 1−3, films were deposited using a focused electron beam in the presence of a constant partial pressure of precursor molecules.[44,45] Under these conditions the steady state concentration of precursor molecules is low ($\theta \ll 0.1$)[44,76] and the size of the deposit is on the submillimeter length scale. These facts preclude the use of most surface analytical techniques capable of monitoring changes in the chemical bonding and composition of the adsorbate layer in situ during electron irradiation. The presence of a partial pressure associated with the EBID precursor also limits the ability of mass spectrometry to identify gas phase species evolved during deposition.

To overcome these experimental limitations, complementary experiments were conducted on nanometer scale thick films of 1,2-DAP physisorbed onto Au substrates under UHV conditions. Results from such studies can provide additional kinetic information on the EBID process as well as new insights into the molecular level events that accompany the electron induced deposition of amorphous carbon nitride films. In these experiments, the initial film thicknesses were ≈3−10 nm, corresponding to at least six molecular layers of adsorbed 1,2-DAP molecules.

Dehydrogenation. Mass spectrometry results shown in Figure 4 reveal that electron irradiation of adsorbed 1,2-DAP produces hydrogen as the dominant gas phase product without any significant loss of volatile species containing nitrogen or carbon. Thus, if electron stimulated desorption of the parent molecule was a significant reaction pathway, peaks at $m/z = 30$ and 43 should be observed due to the $NH_2\text{-}CH_2^+$ and $NH_2\text{-}CH\text{-}CH_3^+$ ions characteristic of gas phase 1,2-DAP,[65] in contrast to our experimental observations (Figure 4b). The absence of any volatile carbon or nitrogen containing species produced during electron irradiation of adsorbed 1,2-DAP is also consistent with the XPS data shown in Figure 8, specifically the lack of change in either the C(1s) and N(1s) XPS areas. Thus, XPS and MS results collectively support the idea that *dehydrogenation is the major chemical transformation that accompanies electron irradiation of molecularly adsorbed 1,2-DAP*. Hydrogen has also been observed as the dominant gas phase product when surface bound amines[77,78] and organic films, including alkanes[79] and self-assembled monolayers,[80−83] are irradiated by incident electrons ranging in energies from 5 eV to 2 keV.

Reaction Kinetics. Because the changes in chemical composition within the adsorbate layer are dominated by the effects of dehydrogenation, temporal changes in the C−H and N−H IR intensities can in principle serve as the basis to probe the electron stimulated reaction kinetics. However, the broadening of the C(1s) and N(1s) XPS spectral envelopes upon irradiation of adsorbed 1,2-DAP, coupled with the observation of nitrile species at longer irradiation times (Figure 7), indicates that dehydrogenation also produces significant changes in the microstructure and local bonding environments within the adsorbate layer. These changes in the film's microstructure will inevitably alter the C−H and N−H oscillator strengths, and as a result, changes in IR band intensities would not provide a reliable quantitative metric of the change in concentration of C−H or N−H bonds during electron beam irradiation. As a result, we have confined our kinetic studies to the effects that external variables (target current and incident electron energy) have on the reaction rate. In this approach, we have taken advantage of the fact that as long as the reaction mechanism remains invariant to changes in these external variables, then for films of similar initial thickness (as determined by the initial C−H and N−H absorbance values), the time required for the C−H or N−H IR areas to decrease by a fixed fraction will be inversely proportional to the rate of C−H or N−H bond cleavage (k_{C-H} or k_{N-H}). This method of determining relative

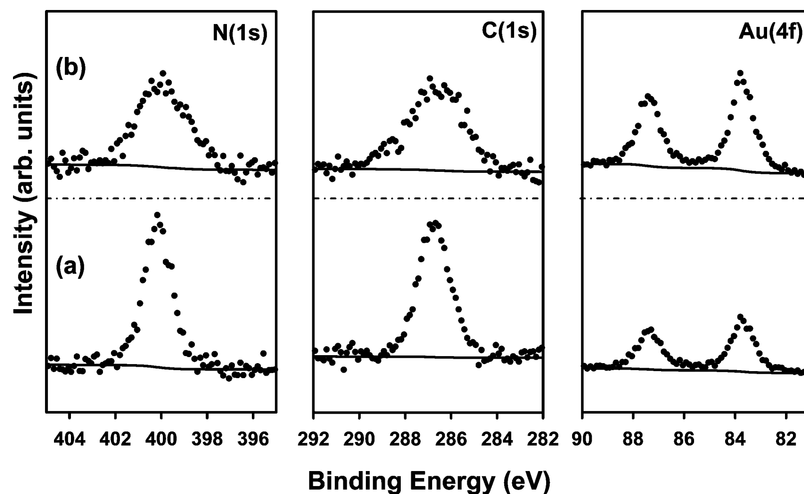

Figure 8. XP spectra of the N(1s), C(1s), and Au(4f) regions of (a) adsorbed 1,2-diaminopropane (3.3 nm thick film) prior to electron irradiation; (b) the same adsorbate layer after electron irradiation (14.6 μA; 1.5 keV; 40 min). To directly compare the effect of electron irradiation the intensity scale has been held constant for each element.

Downloaded by JOHNS HOPKINS UNIV on July 14, 2009
Published on June 15, 2009 on http://pubs.acs.org | doi: 10.1021/jp900966m

reaction rates does not require a detailed knowledge of the elementary reaction steps and is independent of changes that may occur in the N−H or C−H oscillator strengths. In our analysis, we have chosen the irradiation time required for the C−H and N−H IR areas to decrease to half of their initial values ($(C-H)_{t1/2}$ and $(N-H)_{t1/2}$). Thus, $(C-H)_{t1/2} \propto k_{C-H}$ and $k_{N-H} \propto (N-H)_{t1/2}$.

Figure 6a shows that k_{C-H} and k_{N-H} are directly proportional to the target current/electron flux. This indicates that the rate determining step in the loss of C−H and N−H bonds involves a one electron process, consistent with EBID processes. As a function of incident electron energy, Figure 6b reveals that k_{C-H} and k_{N-H} both reach a maximum at $\approx$ 200 eV. Furthermore, analysis of Figures 6a and 6b reveals that the k_{C-H}/k_{N-H} ratio remains constant, both as a function of incident electron energy and flux.

The variation in k_{C-H} and k_{N-H} as a function of the incident electron energy (Figure 6b), with a peak at primary electron energies of $\approx$ 200 eV, is similar to the variation in the secondary electron yield that is observed when solid surfaces are exposed to electron irradiation.[84−86] This suggests that it is the low energy (primarily <20 eV) secondary electrons that are responsible for the electron stimulated reactions observed in the present study. Similar conclusions have also been reached from measurements of deposition yields as a function of incident electron energy in related studies involving the electron induced deposition of amorphous carbon films from gas phase benzene,[75] tungsten from $W(CO)_6$[87,88] and platinum from trimethyl (methyl cyclopentadienyl) platinum(IV) ($MeCpPt(IV)Me_3$).[89] In addition, experiments performed on the electron-induced decomposition of $MeCpPt(IV)Me_3$ adsorbed onto Au substrates have revealed that the decomposition/deposition rate exhibits a similar functional dependence on the incident electron energy to the one observed for 1,2-DAP, with a maximum $\approx$200 eV.[89,90] Given the significant differences in the molecular structure of 1,2-DAP and $MeCpPt(IV)Me_3$, this observation suggests that for both adsorbates decomposition is not initiated by the primary beam, but by the secondary electrons whose yield is maximized when the incident electron energy is $\approx$200 eV. The idea that low energy secondary electrons are principally responsible for the decomposition of adsorbed 1,2-DAP is also consistent with the fact that molecular hydrogen has previously been detected as the dominant gas product produced when organic films are irradiated by low energy electrons.[80,81,83] For surface-bound 1,2-DAP, the importance of reactions involving low energy secondary as opposed to primary electrons is responsible for the pronounced differences in the volatile fragments produced when gas phase and adsorbed 1,2-DAP molecules are exposed to electrons with incident energies >50 eV (see Figure 4).

Hydrogen Production. Based on detailed discussions described in previous studies,[80,81,83] we believe that hydrogen production from adsorbed 1,2-DAP will occur principally from electronically excited anionic species formed by the interaction of secondary electrons ($e^-_{(sec)}$) with the parent molecule

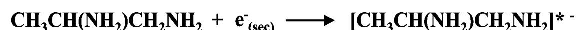

These highly reactive species can produce hydrogen via a direct intramolecular elimination process,[80,81,83] where the excess charge (e^-) may or may not remain in the film

As has been shown in previous studies, an alternative pathway involves the H^- ejection when the excited anionic species decomposes to form a radical.[91,92]

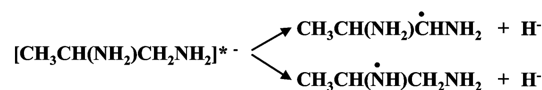

The H^- species can then either escape into vacuum or generate hydrogen via hydrogen or proton abstraction reactions with other adsorbates.[80,93]

Based on this sequence of basic steps, the reactions of secondary electrons with an adsorbate layer consisting of 1,2-DAP molecules will lead to dehydrogenation and the formation of carbon and nitrogen centered radicals. Consistent with our experimental results, this reaction sequence predicts that the loss of both C−H and N−H bonds from the film should be proportional to the incident electron flux, while the ratio of k_{C-H}/k_{N-H} remains independent of the electron flux and incident electron energy.

Formation of Amorphous Carbon Nitride Films. Once formed, the carbon- and nitrogen-centered radicals can participate in cross-linking reactions, forming new C−C and C−N

bonds as an amorphous carbon nitride film develops under the influence of electron irradiation. For example,

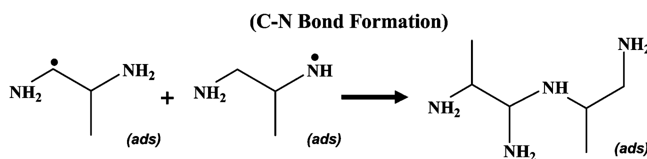

Such a process is analogous to the reactions believed to be responsible for the formation of amorphous carbonaceous films when alkanes and hydrocarbon films are electron irradiated.[82,94]

The idea that a carbon nitride film forms in our UHV studies is supported by the fact that the C(1s) and N(1s) XPS areas remain unchanged upon heating the film to room temperature, under conditions where any lower weight molecular species (including residual 1,2-DAP molecules) would have molecularly desorbed. The ability of 1,2-DAP to act as a precursor for amorphous carbon nitride film formation under the influence of electron irradiation is also consistent with the results presented in Figures 1-3, where films were deposited in the presence of a constant partial pressure of 1,2-DAP.

Another consequence of the cross-linking reactions and the loss of hydrogen is that the film will increase in density under the influence of electron irradiation, with a concomitant decrease in film thickness. Experimentally, this is observed by the increase in intensity of the substrate Au(4f) photoelectrons. For example, in Figure 8, an initially 3.3 nm thick film of adsorbed 1,2-DAP decreases in average thickness by 0.8 nm as a result of electron irradiation, while there is no change in the C(1s) or N(1s) XPS areas.[95]

Formation of Nitrile Species. In parallel with film formation, electron stimulated dehydrogenation continues, leading to the formation of new local bonding environments within the film, as illustrated below:[96]

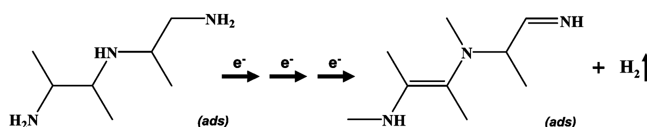

Experimentally, changes in the local bonding environments within the film are consistent with the evolution of both the C(1s) and N(1s) lineshapes. However, the clearest evidence of the film's evolution under the influence of electron irradiation is provided by the appearance of nitrile (C≡N) groups (Figure 7). These new species are observed only after prolonged periods of irradiation when a significant fraction of the initial C−H and N−H bonds have been lost. We postulate that these nitrile species form as a result of dehydrogenation reactions, such as

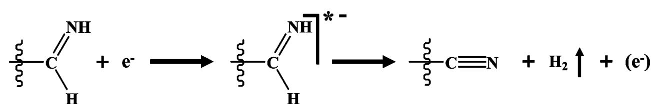

With respect to plasma processes used to deposit amorphous carbon nitride thin films, our results indicate that electron induced reactions at the surface of the growing film could contribute to the formation of chain terminating carbon atoms. Indeed, CN triple bonds have been produced in amorphous carbon nitride films exposed to UV irradiation where low energy electrons would be generated by the interactions of photons with the film.[70] The presence of these terminal carbon atoms in amorphous carbon nitride films have important consequences for materials properties because they disrupt the continuity of the C−N−C bonding network and decrease the film's hardness and wear resistance.[97]

The proposed mechanism for the electron-stimulated formation of amorphous carbon nitride thin films from adsorbed 1,2-DAP is shown in Scheme 1. The overall process is dominated by the effects of C−H and N−H bond cleavage, mediated by reactions of secondary electrons with the adsorbate layer. During the initial stages of the reaction, dehydrogenation is accompanied by the formation of new C−N and C−C bonds as a hydrogenated amorphous carbon nitride (a:C−N(H)) thin film develops. As the electron dose increases, further dehydrogenation leads to the formation of unsaturated NC(sp^2) and NC(sp^3) bonds. We believe that an analogous reaction sequence would also describe the EBID of amorphous carbon nitride films from other volatile nitrogen containing organics. In this context, our results also have implications for the formation of amorphous carbon nitride films known as tholins postulated to form in the atmosphere of Titan as a result of the reactions of amines with reactive species, including electrons.[98,99]

Implications of UHV Studies to Films Deposited in a Partial Pressure of 1,2-DAP. From a practical standpoint, optimal growth rates of amorphous carbon nitride films will require incident electrons with energies close to 200 eV (Figure 6b), due to the optimal yield of secondary electrons. However, it is experimentally difficult to operate a standard focused electron beam below 1 keV. Our UHV studies also suggest that deposition will occur as a result of reactions between carbon- and nitrogen-centered radicals produced by the electron-stimulated decomposition of transiently adsorbed precursor molecules, while the dominant chemical transformation that accompanies film growth is dehydrogenation. Thus, the secondary electrons generated by the primary beam serve not only as the means to initiate film growth, but also to moderate the film's microstructure as a consequence of dehydrogenation. Consequently, we expect that the microstructure of a film deposited under typical EBID conditions will be determined by the partial pressure of the precursor as well as the fluence of secondary

SCHEME 1: Proposed Mechanism for the Production of an Amorphous Carbon Nitride Film from the Electron Beam-Induced Decomposition of 1,2-Diaminopropane

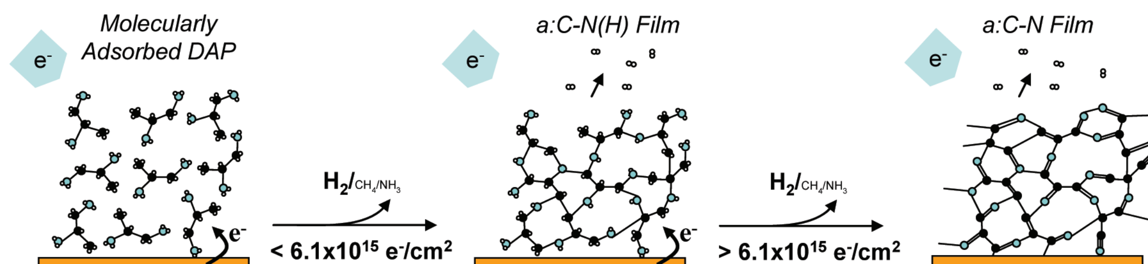

Downloaded by JOHNS HOPKINS UNIV on July 14, 2009
Published on June 15, 2009 on http://pubs.acs.org | doi: 10.1021/jp900966m

electrons. For example, films deposited using a relatively high incident electron flux will be extensively dehydrogenated with higher concentrations of nitrile species. This will have important consequences for the film's material properties.

Results from our UHV studies indicate that the film's ultimate N/C ratio is a reflection of the precursor's chemical composition. However, AES analysis of the amorphous carbon nitride films deposited in Figure 1 indicates that the N/C ratio is less than that of the precursor (Supporting Information, Figure 2). This difference is probably a reflection of the fact that the electron flux in the high-pressure deposition studies (Figures 1−3) is ≈20 times greater than the electron fluxes in the UHV studies (Figures 4−8). In this regard, recent studies on metal deposits formed by electron deposition of organometallic precursors, such as trimethyl (methyl cyclopentadienyl) platinum(IV) (MeCpPt(IV)Me_3), have shown that the metal content in the deposited films is influenced by the incident electron flux,[100] underscoring the complexity of the reaction processes responsible for EBID. Thus, it appears the N/C ratio of electron deposited amorphous carbon nitride films will be influenced by both the precursor's chemical composition and the electron fluence. This has important implications for controlling the properties of a:C−N and a:C−N(H) films, which are sensitive to the film's N/C ratio.[3,101]

Downloaded by JOHNS HOPKINS UNIV on July 14, 2009
Published on June 15, 2009 on http://pubs.acs.org | doi: 10.1021/jp900966m

V. Conclusions

For incident electron energies >40 eV, the decomposition of adsorbed 1,2-DAP molecules is initiated by secondary electrons produced by the interaction of the primary beam with the adsorbate layer and the substrate. The reactions of these low energy secondary electrons with adsorbed 1,2-DAP molecules lead to the evolution of molecular hydrogen and the formation of radicals that cross-link to form a hydrogenated amorphous carbon nitride (a:C−N(H)) thin film. For prolonged periods of electron irradiation, the sustained loss of C−H and N−H bonds continues to change the film's microstructure, including the formation of nitrile groups, as an amorphous carbon nitride (a:C−N) thin film develops. Electron stimulated reaction rates, measured by the loss of C−H and N−H bonds from the adsorbate layer in UHV studies and the increase in film thickness in higher pressure deposition studies are both directly proportional to the incident electron flux, consistent with EBID processes. Experimental evidence suggests that the chemical composition and microstructure of amorphous carbon nitride films deposited by EBID will be influenced by both the chemical composition of the precursor and the electron flux.

Acknowledgment. The authors would like to acknowledge support from the National Science Foundation (#CHE-0616873). We also acknowledge the use of the surface analysis laboratory at Johns Hopkins University.

Supporting Information Available: Secondary electron image of an amorphous carbon nitride file and a representative AES spectra of an amorphous, EBID deposited carbon nitride film. This material is available free of charge via the Internet at http://pubs.acs.org.

References and Notes

(1) Spaeth, C.; Kuhn, M.; Chudoba, T.; Richter, F. *Surf. Coat. Technol.* **1999**, *112*, 140.
(2) Jama, C.; Dessaux, O.; Goudmand, P.; Soro, J.-M.; Rats, D.; von Stebut, J. *Surf. Coat. Technol.* **1999**, *116−119*, 59.
(3) Wei, B.; Zhang, B.; Johnson, K. E. *J. Appl. Phys.* **1998**, *83*, 2491.
(4) Franceschini, D. F.; Achete, C. A.; Freire, J. F. L. *Appl. Phys. Lett.* **1992**, *60*, 3229.
(5) Godet, C.; Conway, N. M. J.; Bouree, J. E.; Bouamra, K.; Grosman, A.; Ortega, C. *J. Appl. Phys.* **2002**, *91*, 4154.
(6) Silva, S. R. P.; Robertson, J.; Amaratunga, G. A. J.; Rafferty, B.; Brown, L. M.; Schwan, J.; Franceschini, D. F.; Mariotto, G. *J. Appl. Phys.* **1997**, *81*, 2626.
(7) Kim, J. H.; Ahn, D. H.; Kim, Y. H.; Baik, H. K. *J. Appl. Phys.* **1997**, *82*, 658.
(8) Hauert, R.; Glisenti, A.; Metin, S.; Goitia, J.; Kaufman, J. H.; Loosdrecht, P. H. M. v.; Kellock, A. J.; Hoffman, P.; White, R. L.; Hermsmeier, B. D. *Thin Solid Films* **1995**, *268*, 22.
(9) Khurshodov, A.; Kato, K.; Daisuke, S. *J. Vac. Sci. Technol., A* **1996**, *A14*, 2935.
(10) Silva, S. R. P.; Amaratunga, G. A. J.; Barnes, J. R. *Appl. Phys. Lett.* **1997**, *71*, 1477.
(11) Li, J.; Zheng, W.; Gu, C.; Jin, Z.; Zhao, Y.; Mei, X.; Mu, Z.; Dong, C.; Sun, C. *Carbon* **2004**, *42*, 2309.
(12) Qin, Z.; Wang, P.; Shen, H.; Mi, L.; Ying, X. *Diamond Relat. Mater.* **2005**, *14*, 1616.
(13) Freire, F. L., Jr.; Franceschini, D. F. *Thin Solid Films* **1997**, *293*, 236.
(14) Jang, H.-k.; Kim, G.; Lee, Y.-S.; Whangbo, S. W.; Whang, C. N.; Yoo, Y.-Z.; Kim, H. G. *J. Korean Phys. Soc.* **1999**, *35*, S399.
(15) Denysenko, I. B.; Xu, S.; Long, J. D.; Rutkevych, P. P.; Azarenkov, N. A.; Ostrikov, K. *J. Appl. Phys.* **2004**, *95*, 2713.
(16) Kim, J. H.; Kim, Y. H.; Choi, D. J.; Baik, H. K. *Thin Solid Films* **1996**, *289*, 79.
(17) Liu, X. W.; Chan, L. H.; Hong, K. H.; Shih, H. C. *Thin Solid Films* **2002**, *420−421*, 212.
(18) Lenardi, C.; Baker, M. A.; Briois, V.; Nobili, L.; Piseri, P.; Gissler, W. *Diamond Relat. Mater.* **1999**, *8*, 595.
(19) Capezzuto, P.; Bruno, G. *Pure Appl. Chem.* **1988**, *60*, 633.
(20) Jacob, W.; Hopf, C.; von Keudell, A.; Meier, M.; Schwarz-Selinger, T. *Rev. Sci. Instrum.* **2003**, *74*, 5123.
(21) Schwarz-Selinger, T.; Meier, M.; Hopf, C.; von Keudell, A.; Jacob, W. *Vacuum* **2003**, *71*, 361.
(22) von Keudell, A.; Jacob, W. *Prog. Surf. Sci.* **2004**, *76*, 21.
(23) Hong, S.-H.; Douai, D.; Berndt, J.; Winter, J. *Plasma Sources Sci. Technol.* **2005**, *14*, 451.
(24) Hayashi, Y.; Kamio, T.; Soga, T.; Kaneko, K.; Jimbo, T. *Diamond Relat. Mater.* **2005**, *14*, 970.
(25) Gyorgy, E.; Mihailescu, I. N.; Baleva, M.; Abrashev, M.; Trifonova, E. P.; Szekeres, A.; Perrone, A. *Mater. Sci. Eng., B* **2003**, *97*, 251.
(26) Liu, D.; Zhou, J.; Fisher, E. R. *J. Appl. Phys.* **2007**, *101*, 023304.
(27) Liu, D.; Fisher, E. R. *J. Vac. Sci. Technol., A* **2007**, *25* (2), 368.
(28) Ennos, A. E. *Br. J. Appl. Phys.* **1954**, *5*, 27.
(29) Watson, J. H. L. *J. Appl. Phys.* **1947**, *18*, 153.
(30) Steward, R. *Phys. Rev.* **1934**, *45*, 488.
(31) Gazzadi, G. C.; Frabboni, S. *J. Vac. Sci. Technol., B* **2005**, *23*, L1.
(32) Toth, M.; Lobo, C. J.; Knowles, W. R.; Phillips, M. R.; Postek, M. T.; Vladar, A. E. *Nano Lett.* **2007**, *7*, 525.
(33) Rack, P. D.; Fowlkes, J. D.; Randolph, S. J. *Nanotechnology* **2007**, *18*, 465602.
(34) Choi, Y. R.; Rack, P. D.; Frost, B.; Joy, D. C. *Scanning* **2007**, *29*, 171.
(35) Utke, I.; Hoffmann, P.; Melngailis, J. *J. Vac. Sci. Technol., B.* **2008**, *26*, 1197.
(36) van Dorp, W. F.; Hagen, C. W. *Appl. Phys.* **2008**, *104* (8), 081301/1-081301/42.
(37) van Dorp, W. F.; van Someren, B.; Hagen, C. W.; Kruit, P.; Crozier, P. A. *Nano Lett.* **2005**, *5*, 1303.
(38) Liang, T.; Stivers, A. Damage-free Mask Repair Using Electron Beam Induced Chemical Reactions. *Proc. IRR* **2002**, *4688*, 375.
(39) Liang, T.; Frendberg, E.; Lieberman, B.; Stivers, A. *J. Vac. Sci. Technol., B* **2005**, *23*, 3101.
(40) Edinger, K.; Becht, H.; Bihr, J.; Boegli, V.; Budach, M.; Hofmann, T.; Koops, H. W. P.; Kuschnerus, P.; Oster, J.; Spies, P.; Weyrauch, B. *J. Vac. Sci. Technol., B* **2004**, *22*, 2902.
(41) Silvis-Cividjian, N.; Hagen, C. W.; Kruit, P. v. d; Stam, M. A.; Groen, H. B. *Appl. Phys. Lett.* **2003**, *82*, 3514.
(42) Utke, I.; Hoffmann, P.; Berger, R.; Scandella, L. *Appl. Phys. Lett.* **2002**, *80*, 4792.
(43) Tanaka, M.; Shimojo, M.; Mitsuishi, K.; Furuya, K. *Appl. Phys. A: Mater. Sci. Process.* **2004**, *78*, 543.
(44) Randolph, S. J.; Fowlkes, J. D.; Rack, P. D. *Crit. Rev. Solid State Mater. Sci.* **2006**, *31*, 55.
(45) Silvis-Cividjian, N.; Hagen, C. W. *Adv. Imaging Electron Phys.* **2006**, *143*, 1.

(46) Hoffman, P.; Utke, I.; Cicoira, F. Limits of 3-D Nanostructures Fabricated by Focused Electron Beam (FEB) Induced Deposition. *Proc. IRR* **2003**, *5023*, 4.

(47) Perry, C. C.; Wolfe, G. M.; Wagner, A. J.; Torres, J.; Faradzhev, N. S.; Madey, T. E.; Fairbrother, D. H. *J. Phys. Chem. B* **2003**, *107*, 12740.

(48) Wagner, A. J.; Vecitis, C.; Fairbrother, D. H. *J. Phys. Chem. B* **2002**, *106*, 4432.

(49) Nakayama, N.; Wilson, S. C.; Stadelmann, L. E.; Lee, H.-L. D.; Cable, C. A.; Arumainayagam, C. R. *J. Phys. Chem. B* **2004**, *108*, 7950.

(50) Kimmel, G. A.; Orlando, T. M. *J. Chem. Phys.* **1994**, *101*, 3282.

(51) Kimmel, G. A.; Orlando, T. M. *Phys. Rev. Lett.* **1996**, *77*, 3983.

(52) Lafosse, A.; Bertin, M.; Domaracka, A.; Pliszka, D.; Illenberger, E.; Azria, R. *Phys. Chem. Chem. Phys.* **2006**, *8*, 5564.

(53) Swiderek, P.; Jäggle, C.; Bankmann, D.; Burean, E. *J. Phys. Chem. C* **2007**, *111*, 303.

(54) Swiderek, P. *Eur. Phys. J. D* **2005**, *35*, 355.

(55) Breton, S.-P.; Michaud, M.; Jäggle, C.; Swiderek, P.; Sanche, L. *J. Chem. Phys.* **2004**, *121*, 11240.

(56) Weeks, L. D.; Zhu, L. L.; Pellon, M.; Haines, D. R.; Arumainayagam, C. R. *J. Phys. Chem. C* **2007**, *111*, 4815.

(57) Harris, T. D.; Lee, D. H.; Blumberg, M. Q.; Arumainayagam, C. R. *J. Phys. Chem.* **1995**, *99*, 9530.

(58) Klyachko, D.; Gantchev, T.; Huels, M. A.; Sanche, L. *Spec. Publ. - R. Soc. Chem.* **1997**, *204*, 85.

(59) Klyachko, D. V.; Huels, M. A.; Sanche, L. *Radiat. Res.* **1999**, *151*, 177.

(60) Wnuk, J. D.; Gorham, J. M.; Rosenberg, S. G.; van Dorp, W. F.; Madey, T. E.; Hagen, C. W.; Fairbrother, D. H. *J. Phys. Chem. C* **2009**, *113*, 287.

(61) Wagner, A. J.; Wolfe, G. M.; Fairbrother, D. H. *J. Chem. Phys.* **2004**, *120*, 3799.

(62) Gorham, J.; Torres, J.; Wolfe, G.; d'Agostino, A.; Fairbrother, D. H. *J. Phys. Chem. B.* **2005**, *109*, 20379.

(63) Carlo, S. R.; Torres, J.; Fairbrother, D. H. *J. Phys. Chem. B* **2001**, *105*, 6148.

(64) Gorham, J. M.; Wnuk, J. D.; Shin, M.; Fairbrother, H. *Environ. Sci. Technol.* **2007**, *41*, 1238.

(65) NIST http://webbook.nist.gov/cgi/cbook.cgi?ID=C78900&Units=SI&Mask=200#Mass-Spec.

(66) Hammerum, S.; Kuck, D.; Derrick, P. J. *Tetrahedron Lett.* **1984**, *25*, 893.

(67) Pouchert, C. *The Aldrich Library of FT-IR Spectra*; Aldrich: Milwaukee, WI, 1997; Vol. 1, p 454.

(68) Hao, J.; Xu, T.; Liu, W. *Mater. Sci. Eng., A* **2005**, *408*, 297.

(69) Khabasheksu, V. N.; Margrave, J. L.; Waters, K.; Schultz, J. A. *Thin Solid Films* **2001**, *381*, 62.

(70) Zhang, M.; Nakayama, Y. *J. Appl. Phys.* **1997**, *82*, 4912.

(71) Inamura, K.; Inoue, Y.; Ikeda, S. *Surf. Sci.* **1985**, *155*, 173.

(72) Riedo, E.; Comin, F.; Chevrier, J.; Bonnot, A. M. *J. Appl. Phys.* **2000**, *88*, 4365.

(73) Johansson, A.; Stafstrom, S. *J. Chem. Phys.* **1999**, *111*, 3203.

(74) Rodil, S. E.; Ferrari, A. C.; Robertson, J.; Milne, W. I. *J. Appl. Phys.* **2001**, *89*, 5425.

(75) Kunze, D.; Peters, O.; Sauerbrey, G. *Z. Angew. Phys.* **1967**, *22*, 69.

(76) Utke, I.; Hoffmann, P.; Meingailis, J. *J. Vac. Sci. Technol., B* **2008**, *26*, 1197.

(77) Davies, B. M.; Craig, J. H., Jr. *Surf. Interface Anal.* **2003**, *35*, 1060.

(78) Lozano, J.; Early, D.; Craig, J. H., Jr.; Wang, P. W.; Kimberlin, K. R. *Surf. Interface Anal.* **2005**, *37*, 366.

(79) Xu, C.; Koel, B. E. *Surf. Sci.* **1993**, *292*, L803.

(80) Rowntree, P. A.; Dugal, P.-C.; Hunting, D.; Sanche, L. *J. Phys. Chem.* **1996**, *100*, 4546.

(81) Olsen, C.; Rowntree, P. A. *J. Chem. Phys.* **1998**, *108*, 3750.

(82) Seshadri, K.; Froyd, K.; Parikh, A. N.; Allara, D. L.; Lercel, M. J.; Craighead, H. G. *J. Chem. Phys.* **1996**, *100*, 15900.

(83) Huels, M. A.; Dugal, P.-C.; Sanche, L. *J. Chem. Phys.* **2003**, *118*, 11168.

(84) Swingler, D. L. *Int. J. Mass Spectrom. Ion Phys.* **1978**, *27*, 359.

(85) Dennison, J. R.; Sim, A.; Thomson, C. D. *IEEE Trans. Plasma Sci.* **2006**, *34*, 2204.

(86) Lin, Y.; Joy, D. C. *Surf. Interface Anal.* **2005**, *37*, 895.

(87) Hoyle, P. C.; Cleaver, J. R. A.; Ahmed, H. *Appl. Phys. Lett.* **1994**, *64*, 1448.

(88) Hoyle, P. C.; Cleaver, J. R. A.; Ahmed, H. *J. Vac. Sci. Technol., B* **1996**, *14* (2), 662.

(89) Botman, A.; deWinter, D. A. M.; Mulders, J. J. L. *J. Vac. Sci. Technol., B* **2008**, *26*, 2460.

(90) van Dorp, W. F.; Wnuk, J. D.; Madey, T. E.; Fairbrother, D. F.; Hagen, C. W. 2009, manuscript in preparation.

(91) du Penhoat, M.-A. H.; Huels, M. A.; Cloutier, P.; Jay-Gerin, J.-P.; Sanche, L. *J. Chem. Phys.* **2001**, *114*, 5755.

(92) du Penhoat, M.-A. H.; Huels, M. A.; Cloutier, P.; Jay-Gerin, J.-P.; Sanche, L. *Phys. Chem. Chem. Phys.* **2003**, *5*, 3270.

(93) Rowntree, P. A. *Surf. Sci.* **1997**, *390*, 70.

(94) Chappas, W. J.; Silverman, J. *Radiat. Phys. Chem.* **1980**, *16*, 437.

(95) This assumes an inelastic mean free path of 2 nm for the Au(4f) photoelectrons.

(96) The frequency of C═C, C−C, or C═N bonds are all below the approx. 1900 cm^{-1} cut off for the InSb detector.

(97) Tabbal, M.; Christidis, T.; Isber, S.; Macrel, P.; El Khakani, M. A.; Chaker, M.; Amassian, A.; Martinu, L. *J. Appl. Phys.* **2005**, *98*, 044310.

(98) Bernard, J.-M.; Quirico, E.; Brissaud, O.; Montagnac, G.; Reynard, B.; McMillan, P.; Coll, P.; Nguyen, M.-J.; Raulin, F.; Schmitt, B. *Icarus* **2006**, *185*, 301.

(99) Imanaka, H.; Khare, B. N.; Elsila, J. E.; Bakes, E. L. O.; McKay, C. P.; Cruikshank, D. P.; Sugita, S.; Matsui, T.; Zare, R. N. *Icarus* **2004**, *168*, 344.

(100) Botman, A.; Hesselberth, M.; Mulders, J. J. L. *Microelectron. Eng.* **2008**, *85*, 1139.

(101) Alba de Sánchez, N.; Carrasco, C.; Prieto, P. *Phys. B (Amsterdam, Neth.)* **2003**, *337*, 318.

JP900966M

Downloaded by JOHNS HOPKINS UNIV on July 14, 2009
Published on June 15, 2009 on http://pubs.acs.org | doi: 10.1021/jp900966m